

# Quantitatively Visualizing Tumor-Related Protease Activity *in Vivo* Using a Ratiometric Photoacoustic Probe

Ling Yin,<sup>‡,||</sup> Hao Sun,<sup>⊥</sup> Hao Zhang,<sup>†</sup> Lei He,<sup>†</sup> Ling Qiu,<sup>#</sup> Jianguo Lin,<sup>#</sup> Huawei Xia,<sup>†</sup> Yuqi Zhang,<sup>†</sup> Shunjun Ji,<sup>\*,‡,§</sup> Haibin Shi,<sup>\*,†,§</sup> and Mingyuan Gao<sup>\*,†,§</sup>

<sup>†</sup>State Key Laboratory of Radiation Medicine and Protection, School for Radiological and Interdisciplinary Sciences (RAD-X) and Collaborative Innovation Center of Radiation Medicine of Jiangsu Higher Education Institutions, Soochow University, Suzhou 215123, P. R. China

<sup>‡</sup>Key Laboratory of Organic Synthesis of Jiangsu Province, College of Chemistry, Chemical Engineering and Materials Science & Collaborative Innovation Center of Suzhou Nano Science and Technology, Soochow University, Suzhou 215123, P. R. China

<sup>§</sup>Institute of Chemistry, Chinese Academy of Sciences, BeiYiJie 2, Zhong Guan Cun, Beijing 100190, P. R. China

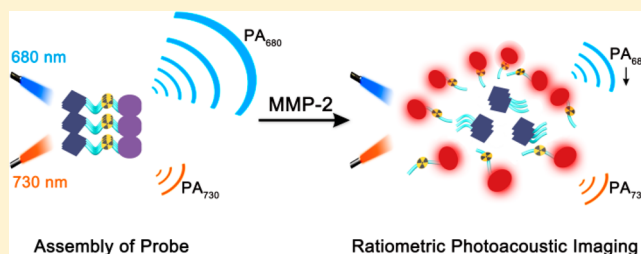
<sup>||</sup>Department of Chemistry and Chemical Engineering, Jining University, Qufu 273155, P. R. China

<sup>⊥</sup>Department of Nuclear Medicine, The First Affiliated Hospital of Soochow University, Suzhou 215006, P. R. China

<sup>#</sup>Key Laboratory of Nuclear Medicine, Ministry of Health, Jiangsu Key Laboratory of Molecular Nuclear Medicine, Jiangsu Institute of Nuclear Medicine, Wuxi 214063, P. R. China

## Supporting Information

**ABSTRACT:** The abnormal expression of tumor-related proteases plays a critical role in cancer invasion, progression, and metastasis. Therefore, it is considerably meaningful to non-invasively assess the proteases' activity *in vivo* for both tumor diagnosis and therapeutic evaluation. Herein, we report an activatable probe constructed with a near-infrared dye (Cy5.5) and a quencher (QSY21) covalently linked through a peptide substrate of matrix metalloproteinases-2 (MMP-2) that was chosen as a model for tumor-associated proteases. Upon cleavage with activated MMP-2, this probe emitted an MMP-2-concentration-dependent fluorescence. Quite unexpectedly, owing to the variation in the aggregation state of both the dye and its quencher as a consequence of the cleavage, the responsive probe presented a dramatic MMP-2-concentration-dependent absorption at around 680 nm, while that at around 730 nm was MMP-2 concentration independent. These features allowed detection of MMP-2 activity via both fluorescence and photoacoustic (PA) imaging *in vitro*, respectively. Moreover, taking the PA signal at 730 nm as an internal reference, the PA signal at 680 nm allowed quantitative detection of MMP-2 expression in breast cancer *in vivo*. We thus envision that our current approach would offer a useful tool for studying the malignant impacts of versatile tumor-associated proteases *in vivo*.



## INTRODUCTION

Abnormal tumor microenvironmental factors such as low extracellular pH, hypoxia, and up-regulated expression of tumor-related proteases are widely accepted as cancer signatures.<sup>1,2</sup> Matrix metalloproteinases (MMPs) are known to be important biomarkers involved in tumorigenesis, invasiveness, metastasis, and angiogenesis of cancers,<sup>3–5</sup> and MMP-2 is one of the most vital MMPs, as it is overexpressed in the majority of solid tumors in, for example, breast,<sup>6</sup> bladder,<sup>7</sup> colon,<sup>8</sup> prostate,<sup>9</sup> and stomach cancers.<sup>10</sup> Therefore, the assessment of MMP-2 activity *in vivo* is of great relevance for clinical diagnosis and therapeutic evaluation of cancers.<sup>11</sup> Non-invasive detection of the protease activity through optical imaging has been reported.<sup>12–26</sup> For example, with the aid of a dual-ratiometric target-triggered fluorescent probe, simultaneous and quantitative mapping of tumor microenvironment protease activity and pH was successfully demonstrated.

Moreover, the overexpression of MMPs was found to be well-correlated, in both time and location, with abnormal pH *in vivo*, and their synergistic effects largely govern the heterogeneous invasion of malignant tumors.<sup>27,28</sup> Apparently, fluorescence imaging offers great potential for visualizing the malignant molecular behaviors. Nevertheless, the limited penetration depth of visible light limits its clinical translation. Fortunately, photoacoustic (PA) imaging, synergistically integrating optical imaging and ultrasound imaging, overcomes the limitations of conventional fluorescence imaging and provides a deeper tissue imaging capacity with high spatial resolution.<sup>29–38</sup>

Although a number of responsive PA probes have recently been reported for non-invasively detecting MMPs *in vivo*,<sup>39–46</sup>

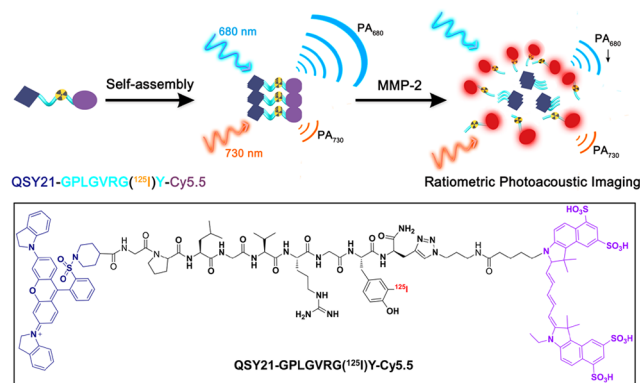
Received: December 21, 2018

Published: January 28, 2019

they do not allow for real-time acquisition of MMPs expression in tumors *in vivo*, which is essential for early tumor diagnosis and evaluation of cancer therapeutic efficacy.

In this study, we report an activatable PA probe that can be used for quantitatively visualizing and analyzing the activity of MMP-2 *in vivo*. As depicted in Scheme 1, a MMP-2 cleavable

### Scheme 1. A Probe for Non-invasively Detecting MMP-2 Activity through Fluorescence/Photoacoustic Imaging



peptide sequence GPLGVRGY was chosen to covalently link Cy5.5 with its quencher QSY21 to establish an activatable structure, QSY21-GPLGVRGY-Cy5.5, that is denoted as QC in the following text. QC is an amphiphilic molecule because QSY21 is more hydrophobic while Cy5.5 is more hydrophilic, so the QC molecules tend to self-assemble into uniform nanoparticles in aqueous solution. Conventional optical characterization revealed that the QC particles in the intact state presented nearly no detectable fluorescence but were readily activated to exhibit strong fluorescence upon incubation with MMP-2. This is reasonable to expect, as QSY21 is an effective quencher for Cy5.5.<sup>47</sup> Quite unexpectedly, the QC nanoparticles also presented a photoacoustic signal at 680 nm that decreased linearly against the concentration of MMP-2, while the PA signal at around 730 nm remained nearly unchanged. This unique feature makes the QC nanoparticles useful for serving as ratiometric photoacoustic imaging probes for quantitatively detecting the MMP-2 activities *in vivo*.

## RESULTS AND DISCUSSION

The probe was synthesized according to our previously reported protocol.<sup>48,49</sup> An alkyne-terminated peptide, GPLGVRGY, was first conjugated to an azido-functionalized Cy5.5 (Cy5.5-N<sub>3</sub>) in DMSO/water (1:1 by vol) by a copper(I)-catalyzed “click” reaction and then reacted with QSY21-NHS (QSY21 carboxylic acid, succinimidyl ester), followed by purification via high-performance liquid chromatography (HPLC) to afford the desired probe QC (Scheme S1 in the Supporting Information). The purity and identity of the probe were confirmed by analytical HPLC and high-resolution mass spectrometry (HR-MS) (Figures S1 and S2). The QC probe was essentially soluble in organic solvent but formed small nanoparticles spontaneously in aqueous buffer. The average size of the resulting nanoparticles is  $9.4 \pm 1.4$  nm, as shown in Figure 1a, according to transmission electron microscopy (TEM) measurements, while the hydrodynamic size was  $\sim 10$  nm, determined through dynamic light scattering (DLS) (Figure S3a). The hydrodynamic size of the resulting

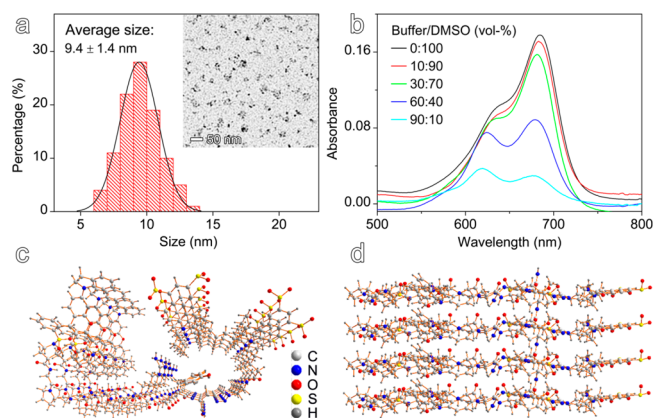


**Figure 1.** (a) Size distribution profile of the QC (40  $\mu$ M) probe particles formed in PBS buffer (pH = 7.4) and a representative TEM image of the probe particles. (b) UV-vis absorption spectra of the QC probe (8  $\mu$ M) in a series of solutions with different buffer:DMSO volume ratios as indicated. (c, d) Self-organized structures of the QC molecules in solid-state particles viewed from different directions according to theoretical calculations.

nanoparticles remained almost unchanged upon storage in phosphate-buffered saline (PBS, pH = 7.4) for more than 30 days (Figure S3b), indicating that not only QC but also the aggregates formed in the aqueous system have very good stability over time. Further measurements revealed that the zeta potential of the QC particles was around  $-26.7$  mV.

The formation of the QC particles was then investigated through absorption spectroscopy. The absorption spectra of QC in DMSO with different volume fractions of buffer were recorded. It is apparent that, with increasing fraction of buffer, the absorbance of QC gradually decreases to a minimum when the buffer fraction is increased to 90%. In the meantime, the absorption shoulder gradually blue-shifts and splits into an evident peak at 619 nm (Figure 1b). To understand these variations in the absorption spectroscopy of QC, the absorption spectra of QSY21 and Cy5.5 in buffer/DMSO with different volume fractions were also investigated. As shown in Figure S4, the absorbance peak of QSY21 dramatically decreased with increasing buffer fraction, which is also accompanied by slight blue-shift of the peak position. All these variations suggest that the solvent polarity has a strong impact on the solubility of QSY21 and that water can induce QSY21 molecules to form aggregates that appear as tiny particles under TEM when the buffer fraction was 90% (Figure S5). In contrast, the variation in the absorption of Cy5.5 was much less evident, although a slight blue-shift in absorption peak position and a little variation in peak intensity was observed, suggesting that the stronger hydrophobicity of QSY21 was the main driving force for QC molecules to form the nanoparticles shown in Figure 1a. The possible aggregating structure of QC molecules was further simulated through calculations. As shown in Figure 1c,d, the QC molecules can be arranged through intermolecular  $\pi$ - $\pi$  stacking via both Cy5.5 and QSY21 groups with an interlayer distance of 5.98 Å, supporting that the strong intermolecular interactions promote the self-assembly of the probe molecules.

To show the responsiveness of the probe in response to MMP-2, a negative control probe (i.e., QSY21-GLALPGY-Cy5.5, denoted as QC control below) was also synthesized according to the same synthetic method mentioned above, based on an alkyne-terminated scrambled peptide,

GLALGPGY, which was not detachable for MMP-2. The results on its purity and molecular structure are given in Figures S1 and S2. It was also experimentally confirmed that QSY21-GLALGPGY-Cy5.5 molecules present aggregation behaviors very similar to those of the QC probes and can thus serve as a suitable control for the following studies. As expected, the fluorescence of QC particle probes can remarkably be activated, showing an on/off ratio up to 44, as given in Figure 2a, upon incubation with activated MMP-2,

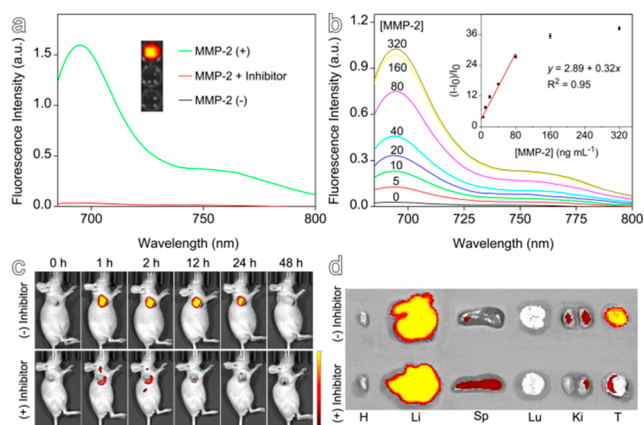


**Figure 2.** (a) Fluorescence spectra of the QC probe ( $4 \mu\text{M}$ ) recorded after incubation with MMP-2 ( $320 \text{ ng mL}^{-1}$ ) [denoted as MMP-2 (+)], a mixture of MMP-2 and its inhibitor GM6001 ( $100 \mu\text{M}$ ) [denoted as MMP-2 + inhibitor] at  $37^\circ\text{C}$  for 2 h in HEPES buffer ( $\text{pH} = 7.4$ ), and the QC probe treated in the absence of MMP-2 [denoted as MMP-2 (-)] (inset: fluorescence images of the above solutions recorded upon excitation at  $675 \text{ nm}$  on an IVIS *in vivo* imaging system). (b) Fluorescence spectra of the QC probe ( $4 \mu\text{M}$ ) recorded after incubation with different concentrations of MMP-2 at  $37^\circ\text{C}$  for 2 h in HEPES buffer (inset: normalized MMP-2 concentration-dependent fluorescence of the QC probe). (c) *In vivo* fluorescence imaging of 4T1 tumor-bearing nude mice injected with the QC probe ( $60 \mu\text{M}$ ,  $200 \mu\text{L}$ ) (top) or GM6001 ( $1.5 \text{ mM}$ ,  $50 \mu\text{L}$ ) 0.5 h after the injection of QC probe (bottom). (d) *Ex vivo* fluorescence images of major organs and tumors dissected from the mice 24 h post injection of the probe (H: heart, Li: liver, Sp: spleen, Lu: lung, Ki: kidney, T: tumor).

while no fluorescence enhancement was determined with the control (Figure S6). In addition, the activation of the QC probe can effectively be inhibited by GM6001, an inhibitor of MMP-2, suggesting that the current QC probe possesses an excellent specificity in response to MMP-2. To characterize the sensitivity of the probe in detecting MMP-2, QC ( $4 \mu\text{M}$ ) was incubated with MMP-2 with concentration ranging from 0 to  $320 \text{ ng mL}^{-1}$ . The fluorescence intensities were carefully recorded and compared. As shown in Figure 2b and Figure S7a, the fluorescence is positively correlated with the concentration of MMP-2 before it gradually reaches a plateau above  $160 \text{ ng mL}^{-1}$ . Further HPLC analysis confirmed that the responsive QC probe can be almost completely digested by MMP-2 through 2 h incubation (Figure S7b). When the MMP-2 concentration is lower than  $80 \text{ ng mL}^{-1}$ , the intensity of the activated fluorescence varies linearly against the MMP-2 concentration ( $R^2 = 0.95$ ) (inset of Figure 2b), according to which a detection limit down to  $0.52 \text{ ng mL}^{-1}$  can be derived (Figure S8).

To further investigate the selectivity of the responsive probe, the QC nanoparticles were treated with different types of

proteins such as BamHI, bovine serum albumin (BSA), Furin, RNase, MMP-9, and MMP-2. The results given in Figure S9a revealed that MMP-9 can also effectively activate the QC probe but with a slightly lower on/off ratio. All this evidence strongly suggests that the current responsive probe can potentially be used for quantitatively detecting the activated MMP-2/-9 with a high sensitivity and selectivity *in vitro*.

The cytotoxicity of the QC probe was assessed through the widely used methyl thiazolyl tetrazolium (MTT) approach. As shown in Figure S9b, the QC probe exhibited negligible cytotoxicity to fibroblast cell line 3T3 and murine breast carcinoma 4T1 cells below  $64 \mu\text{M}$ . The overall cell viability for these two types of cells remained above 80% after they were incubated with the QC probes for 24 h. In the following experiments, 4T1 cells were chosen as MMP-2-positive cancer cells, while 3T3 cells expressing a low level of MMP-2 were taken as a negative control. Figure S10 presents confocal laser scanning microscopy images of 4T1 and 3T3 live cells after being incubated with the QC probes for 8 h. The 3T3 cells exhibit extremely low fluorescence, while 4T1 cells present very strong fluorescence after co-incubation. Moreover, the fluorescence intensity of 4T1 cells could remarkably be suppressed by the MMP-2 inhibitor. Collectively, all the above results demonstrate that the QC responsive probe can specifically be hydrolyzed by MMP-2 secreted by cancer cells *in vitro*, which encouraged us to further evaluate its potential in visualizing MMP-2 activity *in vivo*.

Figure 2c and Figure S11a show series of representative fluorescence images of mice ( $n = 3$ ) bearing 4T1 tumor xenografts, acquired at selected time points after intravenous injection of the QC probe, QC control, or QC probe mixed with the MMP-2 inhibitor, respectively. It is apparent that the 4T1 tumor can clearly be visualized through high signal-to-noise fluorescence. In brief, the fluorescence signal appears 1 h post injection of the QC probe ( $60 \mu\text{M}$ ,  $200 \mu\text{L}$ ) and reaches an intensity maximum approximately 2 h post injection. However, the fluorescence from the control groups of mice receiving the QC control ( $60 \mu\text{M}$ ,  $200 \mu\text{L}$ ) or intratumoral injection of MMP-2 inhibitor ( $1.5 \text{ mM}$ ,  $50 \mu\text{L}$ ) 30 min after the delivery of the QC probe, exhibited greatly lowered intensity (Figures S11b and S12a). Probably due to the nanometer size of the probe particles,<sup>50</sup> liver dominates the biodistribution of the QC probes and presents an evident signal even in the “off” state, where the fluorescence of the QC probe is supposed to be rather weak (Figure 2d and Figure S12b). To further show the pharmacokinetic behavior, the QC probe was labeled with  $^{125}\text{I}$  and then delivered into tumor-bearing mice for single-photon emission computed tomography (SPECT) imaging (Scheme S2). As shown in Figure S12c, the tumor uptake of the  $^{125}\text{I}$ -labeled QC probe became evident 15 min post injection, and then the radioactivity signal gradually increased and reached a maximum with approximately 1.93% ID/g at 2 h post injection (Figure S12d), which is highly consistent with the aforementioned *in vivo* fluorescence imaging results and further suggests that the responsive probe can promptly be activated once within the tumor. This quick response was also directly observed through real-time *in vivo* confocal fluorescence microscopy imaging of the tumorous areas before and after administration of the QC probe (Figures S13 and S14, and Video S1). Collectively, these results well demonstrate that the current responsive probe can potentially be used to visualize the tumor-associated protease *in vivo* for both tumor diagnosis and studies.

According to the strong absorption in the near-infrared regions, both Cy5.5 and its quencher QSY21 can increase the photoacoustic imaging contrast of tumors. Nevertheless, owing to their different hydrophobicity degrees, the cleavage of the peptide linker unavoidably alters the aggregation state of the QC molecules and the energy-transfer efficiency between Cy5.5 and QSY21 to give rise to a variable photoacoustic signal, which may be used for quantifying the expression of MMP-2 *in vivo*. To verify this hypothesis, the absorption spectra of the QC probe were recorded in the presence of different concentrations of MMP-2 in HEPES buffer. As shown in Figure 3a, the intensities of the main absorption peaks of the

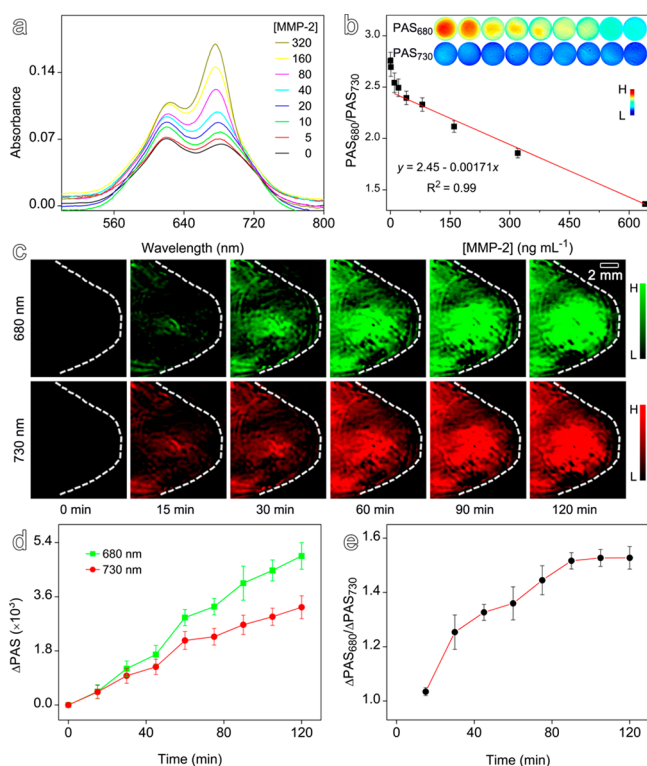


**Figure 3.** (a) UV-vis absorption spectra of the QC probe (8  $\mu\text{M}$ ) recorded after incubation with MMP-2 under different MMP-2 concentrations (ng  $\text{mL}^{-1}$ ). (b) Correlation between the  $\Delta\text{PAS}_{680}/\Delta\text{PAS}_{730}$  of the QC probe (0.25  $\mu\text{M}$ ) and the concentration of MMP-2 recorded at 37  $^{\circ}\text{C}$  after incubation for 2 h (inset: PA images of the QC probe solutions containing different amounts of MMP-2). (c) Temporal photoacoustic images of 4T1 tumor-bearing nude mice injected with the QC probe (60  $\mu\text{M}$ , 200  $\mu\text{L}$ ) recorded under illumination of 680 and 730 nm, respectively. The tumor regions are delineated by white dotted circles. (d) Temporal photoacoustic signal ( $\Delta\text{PAS}$ ) of the tumor site after subtracting the pre-contrasted signal recorded under illumination at 680 and 730 nm, respectively. (e) Temporal ratiometric signal  $\Delta\text{PAS}_{680}/\Delta\text{PAS}_{730}$ .

QC probe at around 620 and 680 nm are greatly increased against the concentration of MMP-2, exhibiting a reverse tendency of the particle aggregation induced by excessive water, as shown in Figure 1b. This is likely due to the release of monomeric Cy5.5, as it is more hydrophilic in comparison the QSY21. Accompanying the increased absorbance, a gradual blue-shift occurring for the 680 nm absorption band leaves the absorbance at 730 nm almost unchanged (Figures S15 and S16). This unique feature thus offers an opportunity to quantitatively determine the MMP-2 level by taking the

photoacoustic signals recorded at 730 nm as an internal reference. To verify this hypothesis, the PA signals of a series of aqueous solutions containing equal amounts of QC probes but different amounts of MMP-2 were recorded after co-incubation for 2 h. The signals recorded under illumination at 680 nm (denoted as  $\text{PAS}_{680}$ ) and 730 nm (denoted as  $\text{PAS}_{730}$ ), respectively, were compared after subtracting the signal recorded from a control solution with no MMP-2 being present. As expected,  $\text{PAS}_{730}$  remains nearly constant, while  $\text{PAS}_{680}$  is dramatically decreased against the concentration of MMP-2. Although the absorption of the QC probe at 680 nm is positively correlated with MMP-2 concentration, the results in Figure 2b indicate that the cleavage of the peptide linker effectively destroys the FRET energy transfer from Cy5.5 to its quencher QSY21. In consequence, the photoenergy absorbed by the QC probe will partly be dissipated in the form of fluorescence rather than heat, which surpasses the positive contribution of the increased absorbance and thus leads to decreased photoacoustic signals.

As  $\text{PAS}_{680}$  is much more sensitive to the concentration of MMP-2, it is plotted against the concentration of MMP-2. To exclude possible interference introduced by variable probe concentration in particular for *in vivo* detection,  $\text{PAS}_{730}$  was adopted as an internal reference. As shown in Figure 3b, the ratio of  $\text{PAS}_{680}/\text{PAS}_{730}$  gradually decreases against the concentration of MMP-2, giving rise to a good linear relationship in MMP-2 concentration range of 10–640 ng  $\text{mL}^{-1}$ , which provides the possibility to quantitatively detect MMP-2 *in vivo* through ratiometric photoacoustic imaging.

In the following animal experiments, the mice bearing subcutaneous 4T1-tumor xenografts ( $n = 3$ ) were imaged upon illumination at 680 and 730 nm, respectively. As the tumors exhibited intrinsic weak PA signals, the intensity increment of PAS ( $\Delta\text{PAS}$  obtained by subtracting the PAS acquired prior to the injection of the QC probe) was determined to show the temporal  $\Delta\text{PAS}$  induced by QC probes through their gradual accumulation in tumor, while  $\Delta\text{PAS}$  induced by the activation of MMP-2 was obtained by taking  $\Delta\text{PAS}_{730}$  as internal reference as mentioned above. As shown in Figure 3c,d, both  $\Delta\text{PAS}_{680}$  and  $\Delta\text{PAS}_{730}$  remarkably increase against time after intravenous injection of the QC probe, which implies that within the initial 2 h of post injection the accumulation of the QC probes keeps increasing (Figure S17). However,  $\Delta\text{PAS}_{680}/\Delta\text{PAS}_{730}$  reaches a plateau 1.5 h post injection after the initial monotonic increase (Figure 3e), suggesting that the amount of the QC probes accumulated within 1.5 h is high enough for reflecting the MMP-2 activity with tumors *in vivo*. In addition, both  $\Delta\text{PAS}_{680}$  and  $\Delta\text{PAS}_{730}$  from the control group of mice intratumorally injected with MMP-2 inhibitor 30 min posterior to the administration of the QC probe were obviously higher than those recorded from the experiment group (Figure S17b,c). More importantly, the ratiometric PA signals ( $\Delta\text{PAS}_{680}/\Delta\text{PAS}_{730}$ ) are enhanced by the inhibitor (Figure S17d), indicating that the activity of MMP-2 is effectively suppressed by the latter.

In light of the above exciting findings, the expression level of MMP-2 in tumors of different sizes was determined for further correlating the ratiometric photoacoustic signal with the expression level of MMP-2 *in vivo*. The PA images of tumors of different sizes were obtained by subtracting the initial PA signal recorded prior to the injection of the probes from that recorded 2 h post injection of the probes. As shown in Figure 4a, the normalized PA signals recorded upon illumination at

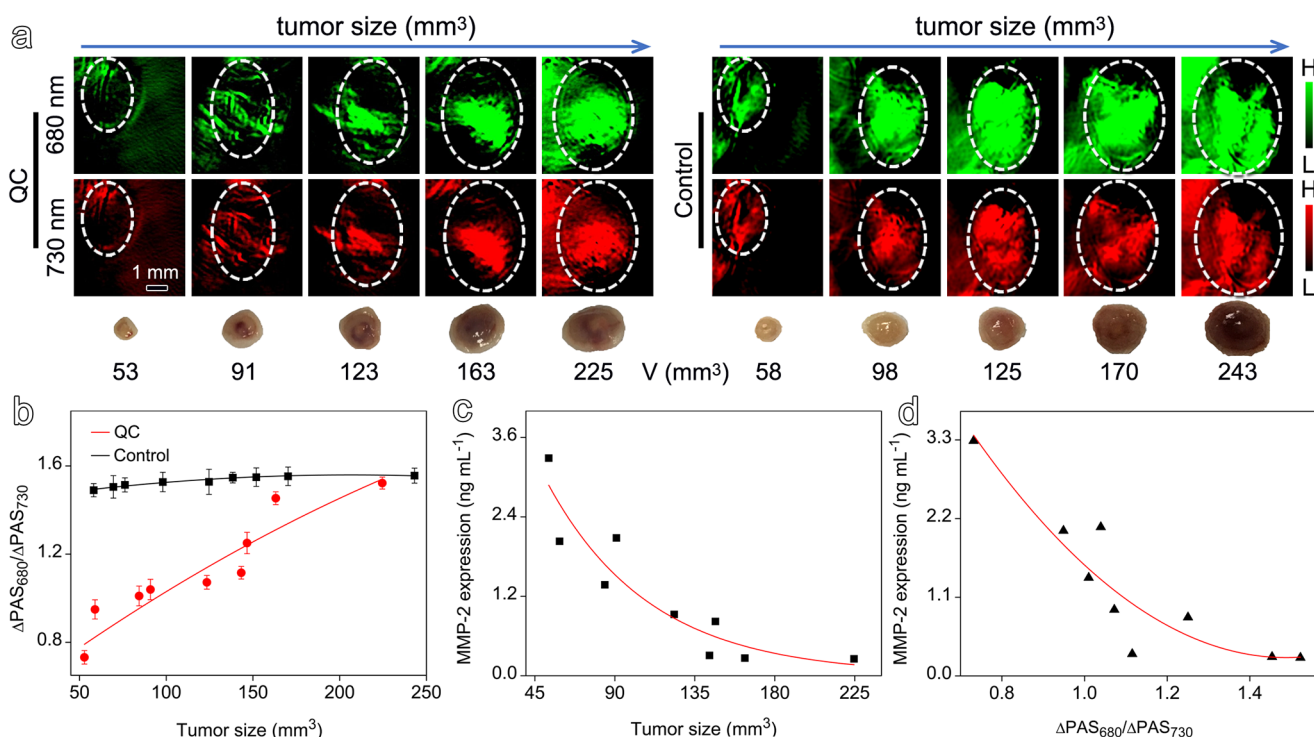


**Figure 4.** (a) PA images of 4T1 tumors of different sizes *in vivo*, recorded 2 h post injection of the QC probe (left, 60  $\mu$ M, 200  $\mu$ L) or its control (right, 60  $\mu$ M, 200  $\mu$ L) through 680 and 730 nm channels, together the photographs of the corresponding tumors harvested right after the PA imaging. Tumor regions are delineated by white dotted circles in the PA images. (b) Ratiometric signal  $\Delta PAS_{680}/\Delta PAS_{730}$  against the tumor size. (c, d) MMP-2 expression levels determined (c) through the conventional tumor-size-dependent method and (d) non-invasively through the  $\Delta PAS_{680}/\Delta PAS_{730}$  signal.

both 680 and 730 nm increase against the tumor size. The ratiometric PA signals ( $\Delta PAS_{680}/\Delta PAS_{730}$ ) of the tumor site for mice receiving QC increase positively against the tumor size in a range of 53–225 mm<sup>3</sup>. However, the  $\Delta PAS_{680}/\Delta PAS_{730}$  keeps a nearly constant for the tumors in a similar size range (58–243 mm<sup>3</sup>) after receiving QC control (Figure 4b), suggesting that the scrambled probe is not responsive to MMP-2 *in vivo*. Figure 4c shows the tumor-size-dependent MMP-2 expression determined through conventional Western blotting assays (more details are given in Figure S18). In brief, the MMP-2 expression decreases against the tumor size, which was also previously observed.<sup>27</sup> This relationship allows us to further quantitatively correlate the integrated ratiometric PA signal with the MMP-2 expression level, as given in Figure 4d. In fact, by activating a responsive fluorescence probe, quantitatively mapping of the expression level of MMPs *in vivo* was previously reported. In comparison with conventional fluorescence imaging, apparently the photoacoustic imaging holds advantages particularly in detection depth. In combination with the ratiometric photoacoustic response of the QC probe, herein we have shown that the quantitative detection of MMP-2 activities *in vivo* is possible. The abnormal expression of tumor-associated proteases is closely related with the malignant behaviors of tumors such as metastasis, apoptosis, and angiogenesis. To non-invasively assess the expression level of the MMPs is undoubtedly meaningful not only for tumor diagnosis, prognosis, and anti-cancer drug screening, but also for in-depth cancer studies.

## CONCLUSION

In summary, we have developed an activatable fluorescence probe for optically detecting the tumor-associated protease

MMP-2. The unexpected ratiometric photoacoustic responsiveness toward MMP-2 provides an opportunity to non-invasively and quantitatively detect the expression level of MMP-2 *in vivo*. We thus believe that this proof-of-concept study may provide a valuable platform for non-invasively investigate the malignant behaviors of tumor-related proteases *in vivo*.

## EXPERIMENTAL SECTION

**General Information.** The peptides GPLGVRGY-Pra and GLALPGY-Pra were synthesized by GL Biochem (Shanghai, China) as requested. Cy5.5 azide was purchased from Click Chemistry Tools (Scottsdale, AZ). QSY21 carboxylic acid, succinimidyl ester (QSY21-NHS) was purchased from Molecular Probes (Eugene, OR). MMP-2 and MMP-9 enzymes were provided by R&D (Minneapolis, MN). RNase was purchased from Thermo Fisher Scientific (Waltham, MA). Furin was obtained from New England Biolabs (Ipswich, MA). BamHI was purchased from Thermo Fisher Scientific (Waltham, MA). BSA was obtained from Sinopharm (Shanghai, China). The MMPs inhibitor GM6001 was purchased from TargetMol (Boston, MA). MTT cell proliferation cytotoxicity assay kit was obtained from Sigma-Aldrich (St. Louis, MO). Hoechst 33342 was purchased from BD (Franklin, NJ). Radionuclide ( $Na^{125}I$ ) was obtained from GMS Pharmaceutical Co., Ltd. (Shanghai, China). M-PER mammalian protein extraction reagent and Pierce ECL Western Blotting substrate were purchased from Thermo Fisher Scientific (Waltham, MA). All chemical reagents used in the synthesis of the probe were obtained from Sigma-Aldrich (St. Louis, MO) and used without any further purification. Milli-Q water with a resistivity above 18 M $\Omega$ -cm was used in the experiments.

HPLC profiles were acquired using 1260 high performance liquid chromatography (Agilent). HR-MS were obtained on a 6230 time-of-flight mass spectrometer and a 6540 UHD accurate-mass quadrupole time-of-flight mass spectrometer (Agilent). UV–vis absorption

spectra were taken on UV spectrometer (UV-3600, Shimadzu). Fluorescence spectra were recorded on fluorescence spectrometer (FLS980, Edinburgh). Dynamic light scattering (DLS) measurements were carried out using a particle size analyzer (Nano ZS90, Malvern). TEM images were taken on an electron microscope (Tecnaï G2 Spirit, FEI). The absorbance was measured using EnSpire multimode plate reader (PerkinElmer). The fluorescence images of probe and mice were acquired with an IVIS Spectrum *in vivo* imaging system (PerkinElmer). The fluorescence micrographs were captured with a fluorescence microscope (FV1200, Olympus). PA imaging was performed with a multispectral optoacoustic tomography (MSOT) scanner (iThera Medical). *In vivo* confocal fluorescence imaging used living confocal microscopy (Cellvizio). SPECT imaging was reconstructed with U-SPECT (MILabsBV).

**Synthesis, Purification, and Characterization of Probe QSY21-GPLGVRGY-Cy5.5.** For synthesis of GPLGVRGY-Cy5.5, 5.01 mg of GPLGVRGY-Pra (0.0055 mmol) was dissolved in 1 mL of DMSO, into which 1 mL of aqueous solution containing 4.93 mg of Cy5.5-N<sub>3</sub> (0.005 mmol), 0.48 mg of CuSO<sub>4</sub> (0.003 mmol), and 1.19 mg of sodium ascorbate (0.006 mmol) was introduced. After reacting for 3 h under continual stirring in the dark at room temperature, the reaction mixture was purified by HPLC to obtain the GPLGVRGY-Cy5.5 followed by the characterization of HR-MS. Calcd. for C<sub>85</sub>H<sub>117</sub>N<sub>19</sub>O<sub>23</sub>S<sub>4</sub><sup>2+</sup>, ([M+2H]<sup>2+</sup>): 949.8721, found ESI-MS: *m/z* 949.8617.

GPLGVRGY-Cy5.5 (1.14 mg, 0.0006 mmol) was subsequently reacted with QSY21-NHS (0.41 mg, 0.0005 mmol) and DIPEA (20  $\mu$ L) in 1 mL of DMF. The reaction mixture was stirred for 5 h in the dark at room temperature, monitored by HPLC. The desired products were finally purified by prep-HPLC and characterized by HR-MS. Calcd. for C<sub>126</sub>H<sub>151</sub>N<sub>22</sub>O<sub>27</sub>S<sub>5</sub><sup>2+</sup>, ([M+2H]<sup>2+</sup>): 1281.9856, found ESI-MS: *m/z* 1281.9746.

**General Procedure for Enzymatic Assay.** *In vitro* enzymatic assays were performed in HEPES buffer (pH = 7.4). Briefly, recombinant MMP-2 (320 ng mL<sup>-1</sup>) was incubated with QC (4  $\mu$ M) or the QC control (4  $\mu$ M) at 37 °C for 2 h. The enzymatic cleavage of probe by MMP-2 was monitored by HPLC. Furthermore, QC (4  $\mu$ M) were incubated with 0, 5, 10, 20, 40, 80, 160, and 320 ng mL<sup>-1</sup> MMP-2 at 37 °C for 2 h in Eppendorf tubes, respectively. The fluorescence intensity was measured with FLS980 spectrometer. The excitation wavelength was fixed at 675 nm, and the emission spectrum was recorded from 685 to 800 nm using a 300  $\mu$ L cuvette.

For competitive experiments, MMP-2 inhibitor (GM6001, 100  $\mu$ M) was first incubated with MMP-2 (320 ng mL<sup>-1</sup>) for 0.5 h followed by the addition of QC (4  $\mu$ M). Meanwhile, the same amount of QC was directly added into the HEPES solution containing 320 ng mL<sup>-1</sup> of MMP-2. After 2 h incubation at 37 °C, the fluorescence intensity was then recorded with FLS980 spectrometer.

To investigate the selectivity of the probe, 4  $\mu$ M of QC was incubated with 320 ng mL<sup>-1</sup> of enzymes (*Bam*HI, BSA, Furin, RNase, MMP-9, MMP-2) at 37 °C for 2 h, respectively. The fluorescence intensity was subsequently determined with FLS980 spectrometer. In addition, the fluorescence imaging performed using an IVIS Spectrum instrument confirmed with the fluorescence spectrum.

**Kinetic Analysis of Probe QC Cleavage.** Kinetic constants of the QC probe in response to MMP-2 were obtained by fitting the experimental data through a nonlinear regression according to the Michaelis–Menten equation,  $V_0 = k_{cat}[E]_0[S]/K_m + [S]$ , with GraphPad Prism software. The Michaelis constant ( $K_m$ ) and the catalytic constant ( $k_{cat}$ ) values were around  $\sim 0.80$   $\mu$ M and  $\sim 0.54$  s<sup>-1</sup> (Figure S23), respectively.

**In Vitro PA Imaging.** PA imaging was performed by MSOT with excitation light of 680–800 nm. Different concentrations of MMP-2 (0, 1, 10, 20, 40, 80, 160, 320, and 640 ng mL<sup>-1</sup>) were incubated with QC (0.25  $\mu$ M) in HEPES buffer followed by PA imaging. PA imaging of free Cy5.5 azide (8  $\mu$ M), free QSY21 (8  $\mu$ M), and QC (8  $\mu$ M) before and after MMP-2 (640 ng mL<sup>-1</sup>) in solutions was also determined on MSOT with excitation light of 680–800 nm.

**Cell Culture.** The murine breast carcinoma cell line 4T1 and murine embryonic fibroblast cell line 3T3 were acquired from the Cell

Bank of the Chinese Academy of Sciences. The 4T1 cells were cultured in RPMI 1640 medium (Hyclone Inc.), supplemented with 10% fetal bovine serum (Hyclone Inc.) and 1% penicillin streptomycin (Beyotime Inc.), at 37 °C in a humidified atmosphere of 5% CO<sub>2</sub>. The 3T3 cells were cultured in DMEM medium (Hyclone Inc.), supplemented with 10% fetal bovine serum (Hyclone Inc.) and 1% penicillin streptomycin (Beyotime Inc.), at 37 °C in a humidified atmosphere of 5% CO<sub>2</sub>. The cells were cultured until 75% confluence was reached, and experiments were performed.

**Cytotoxicity Assay.** The cytotoxicity of probe was measured using commonly MTT assay. The 4T1 cells and 3T3 cells were planted at a density of  $1 \times 10^4$  cells/well in 96-well cell culture plate, respectively. After growing for 24 h, the cells were incubated with different concentrations of QC (0, 2, 4, 8, 16, 32, and 64  $\mu$ M). Then, the cell viability was determined by MTT cell proliferation cytotoxicity assay kit 24 h after the treatments. The absorbance was measured using EnSpire multimode plate reader at a wavelength of 490 nm.

**Confocal Imaging.** The 4T1 cells and 3T3 cells were plated in 8-well plates with a concentration of  $1 \times 10^4$  cells/well, respectively. After growing for 24 h, both groups of cells were incubated with QC (4  $\mu$ M) in the presence and absence of inhibitor GM6001 (100  $\mu$ M). The cell fluorescence imaging was then determined by Hoechst 33342 assay kit 8 h after the treatments. The samples were observed through an FV1200 laser scanning confocal microscope.

**Mice Tumor Model Construction.** Female BALB/c athymic nude mice with body weights of 18–20 g purchased from ChangZhou Cavensla Experimental Animal Technology Co. Ltd. were housed under standard conditions (25  $\pm$  2 °C/60%  $\pm$  10% relative humidity) with 12 h light/dark cycle. The tumors were grafted by subcutaneous inoculation of  $1 \times 10^6$  4T1 cells in about 50  $\mu$ L PBS into the right front flank of each mouse. Fluorescence, SPECT, and PAI studies were carried out when tumor size reached about 50 mm<sup>3</sup>. All animal experiment protocols were compliant with the Animal Ethics Committee of the Soochow University Laboratory Animal Center.

**In Vivo Fluorescence Imaging of Tumors.** QC (60  $\mu$ M, 200  $\mu$ L) was intravenously injected into 4T1 tumor-bearing nude mice via the tail vein with and without 0.5 h posterior intratumoral treatment of inhibitor GM6001 (1.5 mM, 50  $\mu$ L). As control experiment, the QC control (60  $\mu$ M, 200  $\mu$ L) was injected into 4T1 tumor-bearing nude mice via the tail vein. The mice were then anesthetized with 3% isoflurane mixed with oxygen gas (0.5 L/min) and imaged by using an IVIS Spectrum system at different time points. The fluorescence images were finally analyzed with vendor software to separate autofluorescence from chromophore signals through spectral unmixing algorithms.

**In Vivo Confocal Fluorescence Imaging of Tumors.** To verify the feasibility of intravital tumor optical imaging, we performed the *in vivo* confocal fluorescence imaging of subcutaneous 4T1 tumors using living confocal microscopy. The tumor-bearing nude mice were first divided into three groups and then subjected to different treatments, i.e., intravenous injection of QC, blank tumor, intravenous injection of QC, and intratumoral injection of inhibitor GM6001 (1.5 mM, 50  $\mu$ L). Typically, QC (60  $\mu$ M, 200  $\mu$ L) was intravenously injected into the tumor-bearing mice via the tail vein, and the mice were then anesthetized with 3% isoflurane mixed with oxygen gas (0.5 L/min), followed by imaging with living confocal microscopy at different time points.

**Ex Vivo Biodistribution Studies.** For the *ex vivo* biodistribution study, mice were sacrificed at 24 h post-injection with QC (60  $\mu$ M, 200  $\mu$ L), and then the major organs and tumor tissues were carefully harvested and rinsed with PBS buffer (pH = 7.4), placed on black paper, and immediately imaged with an IVIS Spectrum instrument. After that, the tumors were subsequently collected for cryosection and eventually imaged by FV1200 laser scanning confocal microscope.

**Radio-iodination of QC with Chloramine-T Method.** QC was radiolabeled by Na<sup>125</sup>I through the direct chloramine-T method.<sup>51</sup> Briefly, QC (40.0  $\mu$ g) was dissolved in PBS buffer (0.01 M, 200  $\mu$ L, pH = 7.4), labeled with Na<sup>125</sup>I (18.5 MBq, 500  $\mu$ Ci), and then chloramine-T (100  $\mu$ g) in PBS (0.01 M, 10  $\mu$ L, pH = 7.4) was added.

The reaction mixture was incubated for 10 min with shaking at room temperature. The crude reaction was then passed over a C18-SepPak (pretreated first with 95% EtOH and then 0.01 M PBS), washed with 4.0 mL PBS to removed free iodine-125, and then eluted into 1.0 mL of 95% EtOH in yield of 70–80%. After that, the solution was heated to 40 °C for 6 h with shaking to evaporate EtOH and the volume of the solution controlled at 50  $\mu$ L. For imaging, the probe was further diluted in 200  $\mu$ L of PBS.

**In Vivo SPECT Imaging.** 4T1 tumor-bearing nude mice were intravenously injected with  $^{125}\text{I}$ -QC (9.25 MBq, 250  $\mu$ Ci, 200  $\mu$ L) via the tail vein. The whole-body SPECT imaging was performed under general anesthesia by inhalation of 3% isoflurane mixed with oxygen gas (0.5 L/min). The mice were maintained in a prone position on a heated animal bed at 37 °C. The representative SPECT images were acquired at different time points. First, SPECT images were acquired with a 60% energy window peaked at 30 keV, with an acquisition time 15 min per frame. After SPECT acquisition, the animal remained anesthetized, the images were obtained at an X-ray voltage of 55 kVp and anode current of 615  $\mu$ A in accurate mode using full angle, three frames averaging. The projection data were reconstructed with U-SPECT. After SPECT data reconstruction, the images were analyzed using PMOD software (PMOD, version 3.6).

**In Vivo Photoacoustic Imaging.** 4T1 tumor-bearing nude mice were anesthetized by 3% isoflurane mixed with oxygen gas (0.5 L/min) delivered via a nose cone and placed into a water bath to maintain their body temperature at 37 °C. Subsequently, QC (60  $\mu$ M, 200  $\mu$ L) and the QC control (60  $\mu$ M, 200  $\mu$ L) were intravenously subjected by tail vein injection, respectively. In addition, the following experiment was also carried out as a control by intravenously injecting the QC probe (60  $\mu$ M, 200  $\mu$ L) 0.5 h prior to the intratumoral injection of inhibitor GM6001 (1.5 mM, 50  $\mu$ L). The mice were then imaged by MSOT with excitation light of 680–800 nm at different time points. After imaging reconstruction, the probe signal in tumor area was measured by ROI analysis using the MSOT imaging system software package. Tumor volume ( $V$ ) was calculated as follows:  $V$  ( $\text{mm}^3$ ) =  $1/2 \times \text{length (mm)} \times \text{width (mm)}^2$ . The MMP-2 activity in tumors of different sizes was calculated by normalizing the protease activity (obtained by comparing PA signal of 680 and 730 nm) according to the tumor volume.

**Determination of MMP-2 Expression in Vitro.** The expression level of MMP-2 by tumor tissues was determined through Western Blot method. The different size tumor tissues extracted were frozen in liquid nitrogen and stored at  $-80$  °C until use. First, the tissues were ground and homogenized with M-PER mammalian protein extraction reagent. After centrifugation at 10 000 rpm for 10 min at 4 °C, the soluble fraction obtained was subjected to Bradford assay for determining the total protein concentration. The MMP-2 content was then determined as follows. The anti-MMP-2 antibody was immobilized in the well plate upon incubation overnight at 4 °C and rinsed three times with 1 $\times$  PBST buffer. The tissue lysate was then incubated in plate for 60 min at 37 °C and rinsed with 1 $\times$  PBST buffer. Pierce ECL Western Blotting substrate was used to detect the chemiluminescence by Tanon 4200 automatic chemiluminescence image analysis system after exposure and by using the Gel-Pro analyzer software to perform gray analysis quantitatively. By comparison with a MMP-2 standard substance, the MMP-2 expression level was determined and normalized according to the total protein concentration.

## ■ ASSOCIATED CONTENT

### ● Supporting Information

The Supporting Information is available free of charge on the ACS Publications website at DOI: 10.1021/jacs.8b13628.

Experimental details and results on the structural characterization of QC and its control; particle size distribution and absorption spectra of the QC probe particles; TEM images of Cy5.5, QSY21, and QC aggregates formed in the mixtures of HEPES buffer/

DMSO; fluorescence response of QC and its control to MMP-2 and different proteases; cytotoxicity of QC probe; confocal microscopy images of different cells stained with the QC probe; Western Blot results of MMP-2 expression in different size tumors, including Schemes S1 and S2 and Figures S1–S24 (PDF)

Video S1, dynamic process of cell imaging after intravenous injection of the QC probe (AVI)

Video S2, dynamic process of cell imaging after intravenous injection of the QC probe mixed with inhibitor (AVI)

Video S3, dynamic process of cell imaging after intravenous injection of the QC control (AVI)

## ■ AUTHOR INFORMATION

### Corresponding Authors

\*gaomy@iccas.ac.cn

\*hbshi@suda.edu.cn

\*shunjun@suda.edu.cn

### ORCID

Shunjun Ji: 0000-0002-4299-3528

Haibin Shi: 0000-0003-2234-9126

Mingyuan Gao: 0000-0002-7360-3684

### Notes

The authors declare no competing financial interest.

## ■ ACKNOWLEDGMENTS

We acknowledge financial support from the National Key Research and Development Program of China (2018YFA-0208800, 2016YFC0101200), National Natural Science Foundation of China (21572153, 81720108024, 81530057), the Key Research and Development Program of Social Development of Jiangsu Province (BE2018655), the Key Program of Natural Science Foundation of Jiangsu Educational Committee (15KJA310004), the Six Talent Peaks Project of Jiangsu Province (YY-032), the Open Project Program of Jiangsu Provincial Key Laboratory of Radiation Medicine and Protection (KJS1767), a Project Funded by the Priority Academic Program Development of Jiangsu Higher Education Institutions, and the Talent Culturing Plan for Leading Disciplines of University of Shandong Province.

## ■ REFERENCES

- (1) Joyce, J. A.; Pollard, J. W. Microenvironmental regulation of metastasis. *Nat. Rev. Cancer* **2009**, *9* (4), 239–252.
- (2) Turk, B. Targeting proteases: successes, failures and future prospects. *Nat. Rev. Drug Discovery* **2006**, *5* (9), 785–799.
- (3) Tarin, D. Sequential electron microscopical study of experimental mouse skin carcinogenesis. *Int. J. Cancer* **1967**, *2* (3), 195–211.
- (4) Kessenbrock, K.; Plaks, V.; Werb, Z. Matrix metalloproteinases: regulators of the tumor microenvironment. *Cell* **2010**, *141* (1), 52–67.
- (5) Egeblad, M.; Werb, Z. New functions for the matrix metalloproteinases in cancer progression. *Nat. Rev. Cancer* **2002**, *2* (3), 161–174.
- (6) Sheen-Chen, S. M.; Chen, H. S.; Eng, H. L.; Sheen, C. C.; Chen, W. J. Serum levels of matrix metalloproteinase 2 in patients with breast cancer. *Cancer Lett.* **2001**, *173* (1), 79–82.
- (7) Davies, B.; Waxman, J.; Wasan, H.; Abel, P.; Williams, G.; Krausz, T.; Neal, D.; Thomas, D.; Hanby, A.; Balkwill, F. Levels of matrix metalloproteinases in bladder cancer correlate with tumor grade and invasion. *Cancer Res.* **1993**, *53* (22), 5365–5369.

- (8) Stearns, M. E.; Wang, M. Type IV collagenase (M(r) 72,000) expression in human prostate: benign and malignant tissue. *Cancer Res.* **1993**, *53* (4), 878–883.
- (9) Fang, J. M.; Shing, Y.; Wiederschain, D.; Yan, L.; Butterfield, C.; Jackson, G.; Harper, J.; Tamvakopoulos, G.; Moses, M. A. Matrix metalloproteinase-2 is required for the switch to the angiogenic phenotype in a tumor model. *Proc. Natl. Acad. Sci. U. S. A.* **2000**, *97* (8), 3884–3889.
- (10) Hemers, E.; Duval, C.; McCaig, C.; Handley, M.; Dockray, G. J.; Varro, A. Insulin-like growth factor binding protein-5 is a target of matrix metalloproteinase-7: implications for epithelial-mesenchymal signaling. *Cancer Res.* **2005**, *65* (16), 7363–7369.
- (11) Coussens, L. M.; Fingleton, B.; Matrisian, L. M. Matrix metalloproteinase inhibitors and cancer: trials and tribulations. *Science* **2002**, *295* (5564), 2387–2392.
- (12) Blum, A. P.; Kammeyer, J. K.; Rush, A. M.; Callmann, C. E.; Hahn, M. E.; Gianneschi, N. C. Stimuli-responsive nanomaterials for biomedical applications. *J. Am. Chem. Soc.* **2015**, *137* (6), 2140–2154.
- (13) Huang, H.; Lovell, J. F. Advanced functional nanomaterials for theranostics. *Adv. Funct. Mater.* **2017**, *27* (2), 1603524.
- (14) Shanmugam, V.; Selvakumar, S.; Yeh, C. S. Near-infrared light-responsive nanomaterials in cancer therapeutics. *Chem. Soc. Rev.* **2014**, *43* (17), 6254–6287.
- (15) Weissleder, R.; Tung, C. H.; Mahmood, U.; Bogdanov, A., Jr. In vivo imaging of tumors with protease-activated near-infrared fluorescent probes. *Nat. Biotechnol.* **1999**, *17* (4), 375–378.
- (16) Jiang, T.; Olson, E. S.; Nguyen, Q. T.; Roy, M.; Jennings, P. A.; Tsien, R. Y. Tumor imaging by means of proteolytic activation of cell-penetrating peptides. *Proc. Natl. Acad. Sci. U. S. A.* **2004**, *101* (51), 17867–17872.
- (17) Lee, S.; Xie, J.; Chen, X. Activatable molecular probes for cancer imaging. *Curr. Top. Med. Chem.* **2010**, *10* (11), 1135–1144.
- (18) Nguyen, Q. T.; Olson, E. S.; Aguilera, T. A.; Jiang, T.; Scadeng, M.; Ellies, L. G.; Tsien, R. Y. Surgery with molecular fluorescence imaging using activatable cell-penetrating peptides decreases residual cancer and improves survival. *Proc. Natl. Acad. Sci. U. S. A.* **2010**, *107* (9), 4317–4322.
- (19) Zhu, L.; Xie, J.; Swierczewska, M.; Zhang, F.; Quan, Q. M.; Ma, Y.; Fang, X. X.; Kim, K. M.; Lee, S.; Chen, X. Y. Real-time video imaging of protease expression in vivo. *Theranostics* **2011**, *1* (1), 18–27.
- (20) Ryu, J. H.; Lee, A.; Lee, S.; Ahn, C. H.; Park, J. W.; Leary, J. F.; Park, S.; Kim, K.; Kwon, I. C.; Youn, I. C.; Choi, K. W. "One-step" detection of matrix metalloproteinase activity using a fluorogenic peptide probe-immobilized diagnostic kit. *Bioconjugate Chem.* **2010**, *21* (7), 1378–1384.
- (21) Huang, C. W.; Li, Z. B.; Conti, P. S. Radioactive smart probe for potential corrected matrix metalloproteinase imaging. *Bioconjugate Chem.* **2012**, *23* (11), 2159–2167.
- (22) Blum, G.; von Degenfeld, G.; Merchant, M. J.; Blau, H. M.; Bogoy, M. Noninvasive optical imaging of cysteine protease activity using fluorescently quenched activity-based probes. *Nat. Chem. Biol.* **2007**, *3* (10), 668–677.
- (23) Myochin, T.; Hanaoka, K.; Iwaki, S.; Ueno, T.; Komatsu, T.; Terai, T.; Nagano, T.; Urano, Y. Development of a series of near-infrared dark quenchers based on Si-rhodamines and their application to fluorescent probes. *J. Am. Chem. Soc.* **2015**, *137* (14), 4759–4765.
- (24) Lee, S.; Ryu, J. H.; Park, K.; Lee, A.; Lee, S.-Y.; Youn, I.-C.; Ahn, C.-H.; Yoon, S. M.; Myung, S. J.; Moon, D. H.; Chen, X. Y.; Choi, K. W.; Kwon, I. C.; Kim, K. Polymeric nanoparticle-based activatable near-infrared nanosensor for protease determination in vivo. *Nano Lett.* **2009**, *9* (12), 4412–4416.
- (25) Lee, S.; Cha, E. J.; Park, K.; Lee, S. Y.; Hong, J. K.; Sun, I. C.; Kim, S. Y.; Choi, K.; Kwon, I. C.; Kim, K.; Ahn, C. H. A near-infrared-fluorescence-quenched gold-nanoparticle imaging probe for in vivo drug screening and protease activity determination. *Angew. Chem., Int. Ed.* **2008**, *47* (15), 2804–2807.
- (26) Zhang, Y.; So, M. K.; Rao, J. H. Protease-modulated cellular uptake of quantum dots. *Nano Lett.* **2006**, *6* (9), 1988–1992.
- (27) Ma, T. C.; Hou, Y.; Zeng, J. F.; Liu, C. Y.; Zhang, P. S.; Jing, L. H.; Shanguan, D. H.; Gao, M. Y. Dual-ratiometric target-triggered fluorescent probe for simultaneous quantitative visualization of tumor microenvironment protease activity and pH in vivo. *J. Am. Chem. Soc.* **2018**, *140* (1), 211–218.
- (28) Hou, Y.; Zhou, J.; Gao, Z. Y.; Sun, X. Y.; Liu, C. Y.; Shanguan, D. H.; Yang, W.; Gao, M. Y. Protease-activated ratiometric fluorescent probe for pH mapping of malignant tumors. *ACS Nano* **2015**, *9* (3), 3199–3205.
- (29) Wang, X.; Pang, Y.; Ku, G.; Xie, X.; Stoica, G.; Wang, L. V. Noninvasive laser-induced photoacoustic tomography for structural and functional in vivo imaging of the brain. *Nat. Biotechnol.* **2003**, *21* (7), 803–806.
- (30) Ntziachristos, V.; Ripoll, J.; Wang, L. V.; Weissleder, R. Looking and listening to light: the evolution of whole-body photonic imaging. *Nat. Biotechnol.* **2005**, *23* (3), 313–320.
- (31) Pu, K. Y.; Shuhendler, A. J.; Jokerst, J. V.; Mei, J. G.; Gambhir, S. S.; Bao, Z. N.; Rao, J. H. Semiconducting polymer nanoparticles as photoacoustic molecular imaging probes in living mice. *Nat. Nanotechnol.* **2014**, *9* (3), 233–239.
- (32) Lyu, Y.; Fang, Y.; Miao, Q.; Zhen, X.; Ding, D.; Pu, K. Intraparticle molecular orbital engineering of semiconducting polymer nanoparticles as amplified theranostics for in vivo photoacoustic imaging and photothermal therapy. *ACS Nano* **2016**, *10* (4), 4472–4481.
- (33) Cheng, X. J.; Sun, R.; Yin, L.; Chai, Z. F.; Shi, H.; Gao, M. Y. Light-triggered assembly of gold nanoparticles for photothermal therapy and photoacoustic imaging of tumors in vivo. *Adv. Mater.* **2017**, *29* (6), 1604894.
- (34) Miao, Q. Q.; Xie, C.; Zhen, X.; Lyu, Y.; Duan, H. W.; Liu, X. G.; Jokerst, J. V.; Pu, K. Y. Molecular afterglow imaging with bright, biodegradable polymer nanoparticles. *Nat. Biotechnol.* **2017**, *35* (11), 1102–1110.
- (35) Lyu, Y.; Xie, C.; Chechetka, S. A.; Miyako, E.; Pu, K. Y. Semiconducting polymer nanobioconjugates for targeted photothermal activation of neurons. *J. Am. Chem. Soc.* **2016**, *138* (29), 9049–9052.
- (36) Miao, Q.; Pu, K. Emerging designs of activatable photoacoustic probes for molecular imaging. *Bioconjugate Chem.* **2016**, *27* (12), 2808–2823.
- (37) Weber, J.; Beard, P. C.; Bohndiek, S. E. Contrast agents for molecular photoacoustic imaging. *Nat. Methods* **2016**, *13* (8), 639–650.
- (38) Jiang, Y.; Pu, K. Advanced photoacoustic imaging applications of near-infrared absorbing organic nanoparticles. *Small* **2017**, *13* (30), 1700710.
- (39) Levi, J.; Kothapalli, S. R.; Ma, T. J.; Hartman, K.; Khuri-Yakub, B. T.; Gambhir, S. S. Design, synthesis, and imaging of an activatable photoacoustic probe. *J. Am. Chem. Soc.* **2010**, *132* (32), 11264–11269.
- (40) Levi, J.; Kothapalli, S. R.; Bohndiek, S.; Yoon, J. K.; Dragulescu-Andrasi, A.; Nielsen, C.; Tisma, A.; Bodapati, S.; Gowrishankar, G.; Yan, X. R.; Chan, C.; Starcevic, D.; Gambhir, S. S. Molecular photoacoustic imaging of follicular thyroid carcinoma. *Clin. Cancer Res.* **2013**, *19* (6), 1494–1502.
- (41) Razansky, D.; Harlaar, N. J.; Hillebrands, J. L.; Taruttis, A.; Herzog, E.; Zebregts, C. J.; van Dam, G. M.; Ntziachristos, V. Multispectral optoacoustic tomography of matrix metalloproteinase activity in vulnerable human carotid plaques. *Mol. Imaging Biol.* **2012**, *14* (3), 277–285.
- (42) Yang, K.; Zhu, L.; Nie, L. M.; Sun, X. L.; Cheng, L.; Wu, C. X.; Niu, G.; Chen, X. Y.; Liu, Z. Visualization of protease activity in vivo using an activatable photo-acoustic imaging probe based on CuS nanoparticles. *Theranostics* **2014**, *4* (2), 134–141.
- (43) Zhang, D.; Qi, G. B.; Zhao, Y. X.; Qiao, S. L.; Yang, C.; Wang, H. In situ formation of nanofibers from purpurin18-peptide conjugates and the assembly induced retention effect in tumor sites. *Adv. Mater.* **2015**, *27* (40), 6125–6130.

(44) Li, L. L.; Ma, H. L.; Qi, G. B.; Zhang, D.; Yu, F.; Hu, Z.; Wang, H. Pathological-condition-driven construction of supramolecular nanoassemblies for bacterial infection detection. *Adv. Mater.* **2016**, *28* (2), 254–262.

(45) Xie, C.; Zhen, X.; Lyu, Y.; Pu, K. Nanoparticle regrowth enhances photoacoustic signals of semiconducting macromolecular probe for in vivo imaging. *Adv. Mater.* **2017**, *29* (44), 1703693.

(46) Reinhardt, C. J.; Zhou, E. Y.; Jorgensen, M. D.; Partipilo, G.; Chan, J. A ratiometric acoustogenic probe for in vivo imaging of endogenous nitric oxide. *J. Am. Chem. Soc.* **2018**, *140* (3), 1011–1018.

(47) Kabelác, M.; Zimandl, F.; Fessler, T.; Chval, Z.; Lankas, F. A comparative study of the binding of QSY 21 and Rhodamine 6G fluorescence probes to DNA: structure and dynamics. *Phys. Chem. Chem. Phys.* **2010**, *12* (33), 9677–9684.

(48) Yu, Z. H.; Luan, F. J.; Leng, X.; Shi, Y. X.; Wang, J.; Yin, L.; He, L.; Shi, H. B.; Chen, W. C. A fluorogenic probe for sensitive detection of MMP-2/9 activities in clinical colorectal cancer tissues. *Kexue Tongbao* **2018**, *63* (3), 318–326.

(49) Shi, H.; Kwok, R. T. K.; Liu, J.; Xing, B.; Tang, B. Z.; Liu, B. Real-time monitoring of cell apoptosis and drug screening using fluorescent light-up probe with aggregation-induced emission characteristics. *J. Am. Chem. Soc.* **2012**, *134* (43), 17972–17981.

(50) Perrault, S. D.; Walkey, C.; Jennings, T.; Fischer, H. C.; Chan, W. C. W. Mediating tumor targeting efficiency of nanoparticles through design. *Nano Lett.* **2009**, *9* (5), 1909–1915.

(51) Chen, L.; Chen, J. Y.; Qiu, S. S.; Wen, L.; Wu, Y.; Hou, Y.; Wang, Y.; Zeng, J. F.; Feng, Y.; Li, Z.; Shan, H.; Gao, M. Y. Biodegradable nanoagents with short biological half-life for SPECT/PAI/MRI multimodality imaging and PTT therapy of tumors. *Small* **2018**, *14* (4), 1702700.